NANO LETTERS
Cite This: Nano Lett. XXXX, XXX, XXX−XXX
Letter
pubs.acs.org/NanoLett

Cation-Dependent Light-Induced Halide Demixing in Hybrid Organic−Inorganic Perovskites

Carolin M. Sutter-Fella,*[,†,‡] Quynh P. Ngo,[§,‡] Nicola Cefarin,[†,⊥] Kira L. Gardner,[#] Nobumichi Tamura,[▽] Camelia V. Stan,[▽] Walter S. Drisdell,[†,∥] Ali Javey,[§,‡] Francesca M. Toma,[†] and Ian D. Sharp*[,†,○]

[†]Chemical Sciences Division, Lawrence Berkeley National Laboratory, Berkeley, California 94720, United States
[‡]Materials Sciences Division, Lawrence Berkeley National Laboratory, Berkeley, California 94720, United States
[§]Electrical Engineering and Computer Sciences, University of California, Berkeley, California 94720, United States
[∥]Joint Center for Artificial Photosynthesis, Lawrence Berkeley National Laboratory, Berkeley, California 94720, United States
[⊥]Department of Physics, Graduate School of Nanotechnology, University of Trieste, 34127 Trieste, Italy
[#]Cyclotron Road, Lawrence Berkeley National Laboratory, Berkeley, California 94720, United States
[▽]Advanced Light Source, Lawrence Berkeley National Laboratory, Berkeley, California 94720, United States
[○]Walter Schottky Institut and Physik Department, Technische Universität München, 85748 Garching, Germany

Supporting Information

ABSTRACT: Mixed cation metal halide perovskites with increased power conversion efficiency, negligible hysteresis, and improved long-term stability under illumination, moisture, and thermal stressing have emerged as promising compounds for photovoltaic and optoelectronic applications. Here, we shed light on photoinduced halide demixing using in situ photoluminescence spectroscopy and in situ synchrotron X-ray diffraction (XRD) to directly compare the evolution of composition and phase changes in $CH(NH_2)_2CsPb$-halide (FACsPb-) and CH_3NH_3Pb-halide (MAPb-) perovskites upon illumination, thereby providing insights into why FACs-perovskites are less prone to halide demixing than MA-perovskites. We find that halide demixing occurs in both materials. However, the I-rich domains formed during demixing accumulate strain in FACsPb-perovskites but readily relax in MA-perovskites. The accumulated strain energy is expected to act as a stabilizing force against halide demixing and may explain the higher Br composition threshold for demixing to occur in FACsPb-halides. In addition, we find that while halide demixing leads to a quenching of the high-energy photoluminescence emission from MA-perovskites, the emission is enhanced from FACs-perovskites. This behavior points to a reduction of nonradiative recombination centers in FACs-perovskites arising from the demixing process and buildup of strain. FACsPb-halide perovskites exhibit excellent intrinsic material properties with photoluminescence quantum yields that are comparable to MA-perovskites. Because improved stability is achieved without sacrificing electronic properties, these compositions are better candidates for photovoltaic applications, especially as wide bandgap absorbers in tandem cells.

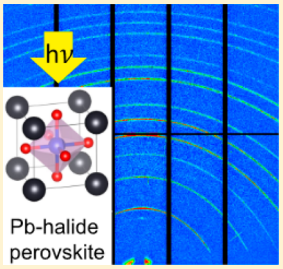

KEYWORDS: *Metal halide perovskite, halide demixing, cation variation, photoluminescence, in situ characterization*

Hybrid metal halide perovskites have recently garnered intense research interest for solar energy conversion[1,2] and optoelectronic applications[3] due to their excellent properties, such as defect tolerance,[4] long minority carrier lifetimes,[5,6] and high photoluminescence quantum yields.[5,7] Their general crystal structure is described by ABX_3, typically comprising a monovalent organic cation A (e.g., $CH_3NH_3^+$ [MA], $CH(NH_2)_2^+$ [FA], or inorganic Cs^+), a divalent metal cation B (Pb^{2+}, Sn^{2+}), and a monovalent anion X (I^-, Br^-, Cl^-). Of particular interest is the wide tunability of the optical bandgap of these materials with halide composition, which makes them attractive wide bandgap semiconductors for use as top cells in tandem photovoltaics.[8−10] For example, alloying of $MAPbI_3$ with Br (i.e., $MAPb(I_{1-x}Br_x)_3$) widens the bandgap from ∼1.6 eV (pure I) to ∼2.3 eV (pure Br).[11] However, photoinduced reversible halide demixing in which phase segregation into I-rich and Br-rich domains occurs under illumination has been reported for $MAPb(I_{1-x}Br_x)_3$ with $0.2 < x < 1$.[12,13] Such phase separation leads to a local reduction of the bandgap and trapping of charge carriers in the I-rich regions. The result is a significant loss of performance in wide bandgap photovoltaic devices due to reduced open-circuit voltage and short circuit current.[14]

Despite the importance of overcoming halide demixing for achieving stable perovskite-based photovoltaic devices, there remains uncertainty about the underlying mechanism(s). Currently, strain- or carrier-induced lattice distortion,[15]

Received: February 7, 2018
Revised: April 16, 2018
Published: April 30, 2018

DOI: 10.1021/acs.nanolett.8b00541
Nano Lett. XXXX, XXX, XXX−XXX

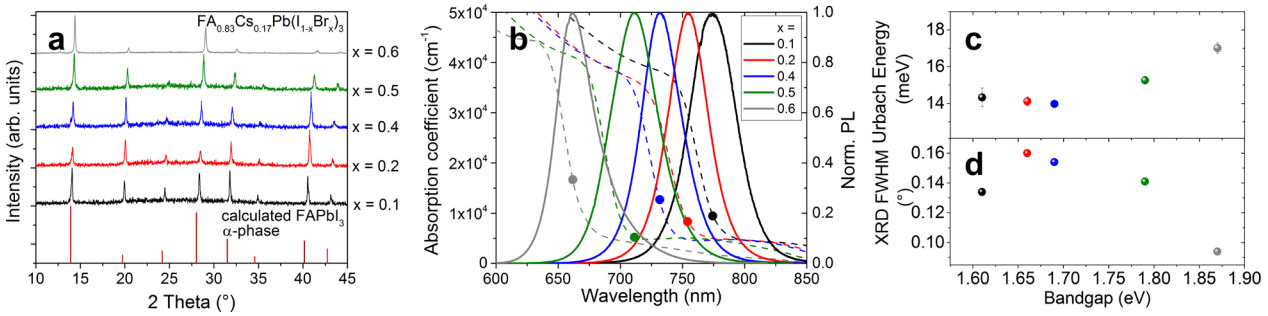

Figure 1. (a) X-ray diffraction patterns of the $FACsPb(I_{1-x}Br_x)_3$ thin films, together with the calculated reference pattern for the alpha (black) $FAPbI_3$ perovskite phase.[19] (b) Absorption coefficient (dashed lines) and PL spectra (solid lines) of the samples studied. The filled circles illustrate the position of the PL maximum with respect to the absorption onset. (c) Urbach energies extracted from the low-energy PL tail as a function of the bandgap. Error bars in *y*-axis represent the standard deviation caused by spectral fluctuations (see Supporting Information, Figure S2) averaging three different spots per sample. (d) fwhm of the (100) X-ray diffraction peak as a function of the bandgap. The color coding in (c,d) is the same as for panels (a,b).

compositional inhomogeneity,[16] defect-mediated halide migration,[13,15,17] and crystal domain size[18] are actively considered as contributing to halide segregation. In particular, Bischak et al. propose that halide demixing is a consequence of localized strain generated from the interaction of charge carriers with the lattice (polaron formation).[15] In this respect, they find that the combination of mobile halides, long charge carrier lifetimes, and significant electron−phonon coupling are prerequisites for halide demixing.[15] In a different study, Barker et al. suggest that defect-assisted halide ion migration away from the illuminated surface with a slower hopping rate of iodide and a potential dependence on charge carrier generation gradients results in formation of I-rich regions at the surface.[13] Finally, Rehman et al. report that short-range crystalline order facilitates halide demixing, possibly by releasing lattice strain between I-rich and Br-rich domains.[18] In this explanation, they argue that halide segregation in a single crystal would cause significant lattice strain that may not be energetically favorable, whereas at grain boundaries lattice strain could be more easily accommodated.[18] Importantly, halide demixing is a complex phenomenon and these hypothesized mechanisms are not necessarily mutually exclusive. In addition, vacancy-mediated halide migration is a requirement for demixing processes and thus a reduction of defect concentrations and rapid diffusion channels is expected to improve stability under illumination.[15,17]

A potential strategy to circumvent halide demixing is by substitution of the A cation. However, alternative monovalent cations, for example pure FA-[19] and Cs-perovskites,[20] are not stable at room temperature and slowly convert to the yellow nonperovskite phase under ambient conditions. Fortunately, the simultaneous incorporation of MA and Br in $FAPbI_3$ perovskites serves to stabilize the perovskite (i.e., alpha) phase,[21] possibly due to a larger dipole interaction of the smaller MA cation with the PbI_6 octahedra.[22] As an indication of the high material quality of mixed cation perovskites, the first reported power conversion efficiency of metal halide perovskite solar cells exceeding 20% was demonstrated with a $MAFAPb(I_{1-x}Br_x)_3$ composition.[23] Calculations suggest that Cs and Rb are more efficient than MA for stabilization of the FA-perovskite phase[24] and first-principles computations show that the perovskite phase stabilization by mixing the A-cations stems from entropic gains.[20] Indeed, $FACsPb(I_{1-x}Br_x)_3$ perovskites have been confirmed by recent reports to exhibit substantially improved stability under illumination,[25,26] moisture,[25] and thermal stressing.[26] A recent review by Ono et al. summarizes the plentiful chemical perovskite compositions (see also ref 27), their solar cell performance, and stability.[28] Since research efforts have mostly been focused on MA-based perovskites and there remains uncertainty about the underlying mechanism(s) of halide demixing in high Br-concentration lead halide perovskites, direct comparison of the more stable $FACsPb(I_{1-x}Br_x)_3$ to light-sensitive MA-perovskites provides opportunity to improve understanding of the nature of such instabilities. Elucidation of the mechanism(s) responsible for reversible photoinduced halide demixing is essential for devising strategies for overcoming these processes and developing more stable mixed halide perovskites.

This paper addresses light-induced halide demixing in hybrid high Br-concentration lead halide perovskites as a function of cation composition. We use in situ photoluminescence and in situ synchrotron X-ray diffraction measurements to probe the differences of halide demixing in FACs- and MA-perovskites. The benefit of using synchrotron radiation for X-ray diffraction is its several orders of magnitude higher flux and brilliance, which allows for significantly shorter data collection time enabling in situ experimentation. Our findings provide mechanistic insights into the enhanced stability against halide demixing in high Br-concentration FACs-perovskites. Although light-induced halide demixing is observed to occur in these FACs-perovskites (shown by photoluminescence), synchrotron X-ray diffraction reveals the absence of peak asymmetry or peak splitting. This suggests that FACs-perovskites accumulate strain during halide demixing, whereas strain is relaxed in MA-perovskites. Such accumulated strain is expected to increase the free energy for the demixed state and the inability of the system to relax represents a stabilizing force for high Br FACs-compounds. In both FACs- and MA-perovskites, the dominant photocarrier recombination behavior is similar with respect to the low-energy emission but fundamentally different with respect to the high-energy emission. One hypothesis to explain this high-energy emission PL increase in FACs-perovskites could be the reduction of nonradiative recombination centers arising from the demixing process and buildup of strain upon illumination compared to the quenching that is observed in MA-perovskites where strain relaxes and charge carriers are funneled to the low-energy regions. Beyond better stability, FACsPb-halide perovskites exhibit excellent intrinsic material properties, as determined by photoluminescence quantum yield measurements. These results indicate that enhanced stability is achieved alongside reduced nonradiative recombination in

DOI: 10.1021/acs.nanolett.8b00541
Nano Lett. XXXX, XXX, XXX−XXX

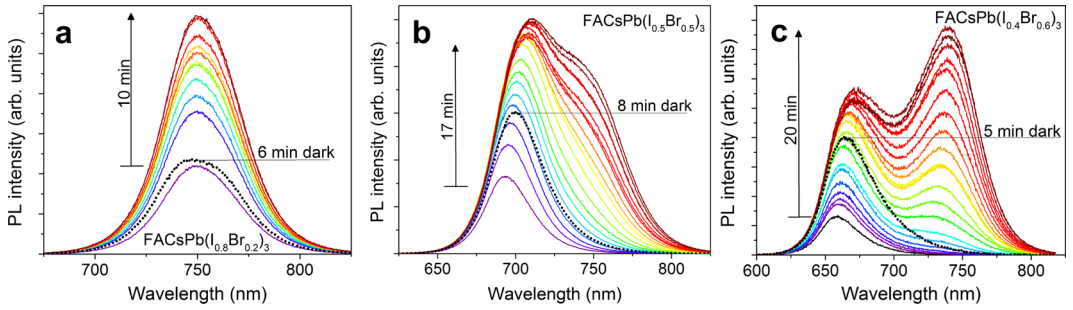

Figure 2. Time evolution of steady-state PL spectra of $FACsPb(I_{0.8}Br_{0.2})_3$ (a), $FACsPb(I_{0.5}Br_{0.5})_3$ (b), and $FACsPb(I_{0.4}Br_{0.6})_3$ (c) thin films taken at ~50 mW/cm^2 illumination density collected in 1 min increments.

FACs-perovskites, thus making them particularly promising wide bandgap semiconductors for optoelectronic applications.

$MAPb(I_{1-x}Br_x)_3$ and $FA_{0.83}Cs_{0.17}Pb(I_{1-x}Br_x)_3$ (in the following shortened to FACsPb-halide or FACs-perovskite) perovskite thin films on glass substrates were fabricated with varying I/(I + Br) ratio by solution processing (see Supporting Information for details) and coated with PMMA to avoid direct contact with atmosphere and possible degradation (compare Figure S1). In FACsPb-halide perovskites, the Cs content of 17% is chosen in accordance with recent work by Rehman et al.[18] Attempts to synthesize films in a wider composition space with respect to Cs/(Cs + FA)-ratio and halide-content (including Cl) resulted either in a nonperovskite phase or less stable behavior under illumination (Supporting Information, Table S1).

Structural and optical properties of $FACsPb(I_{1-x}Br_x)_3$ films with increasing Br content are presented in Figure 1. X-ray diffraction (XRD) measurements confirm crystallization in the alpha (black perovskite) phase[19] (Figure 1a). The samples show high-absorption coefficients of $>4 \times 10^4$ cm^{-1} above the bandgap (Figure 1b, dashed lines) and increasing bandgaps (E_g) from 1.61 eV $\leq E_g \leq$ 1.87 eV for $0.1 \leq x \leq 0.6$. The bandgaps were experimentally estimated using Tauc analysis of the absorption coefficients extracted from UV−vis spectroscopy. We note that bandgap extraction from Tauc analysis is only valid if excitonic effects are negligible, otherwise the obtained values are slightly underestimated.[29] The photoluminescence (PL) spectra are overlaid with the corresponding absorption spectra (Figure 1b) and show the PL maximum to be slightly blueshifted with respect to the absorption onsets with the most pronounced shift of ~20 nm occurring for the sample with the highest Br content in this study (x = 0.6). Such a behavior could be related to the exciton binding energy, self-absorption, or Coulomb interaction. Figure 1c illustrates the Urbach energies extracted from the PL spectra using the van Roosbroeck−Shockley equation, where the optical emission rate is linked to the absorption coefficient (details are given in the Supporting Information and Figure S3).[30,31] To account for inhomogeneities (see Supporting Information, Figure S2), Urbach energies were extracted from three independent PL measurements taken across each sample and the standard deviation is included. We also show the Urbach energies of MAPb-halide samples for comparison (Supporting Information, Figure S4).[12,32] The Urbach energy, which provides a qualitative indication of the crystal lattice distortion caused by defects, dislocations, strain, and impurities, is found to be small, especially considering the fact that these samples are processed at low temperature with simple solution processing, and confirms high crystal quality. For all I/(I + Br)-compositions investigated, the Urbach energy does not exceed 17 meV, which is consistent with the literature value[26] of 16.5 meV for the single composition $FACsPb(I_{0.6}Br_{0.4})_3$. Furthermore, we find that the trend in Urbach energy with increasing x is similar for MAPb- and FACsPb-halide perovskites (Supporting Information, Figure S4). Figure 1d shows the full width at half-maximum (fwhm) extracted from the (100)-X-ray diffraction peak of FACsPb-halide perovskites as a function of halide content. Sharp diffraction peaks are observed for all compositions with highest crystallinity, corresponding to smallest fwhm, observed for the highest Br content (x = 0.6). As shown in Figure S5 (Supporting Information), MA-samples are characterized by somewhat smaller XRD fwhm than FACs-samples, indicating larger domain sizes for MAPb-halide perovskites compared to FACs-perovskites.

The intensity of the PL spectra of FACsPb-halides gradually increases (within minutes) upon monochromatic illumination with an Ar-ion laser (514.5 nm excitation wavelength, ~50 mW/cm^2) as depicted in Figure 2. This photoinduced increase is reversible when remeasuring the samples after they were kept in the dark for several minutes. A rise in PL signal (within seconds[15,33]) has been observed previously for low Br-content/pure I MA-perovskites (i.e., phase-stable compositions) and is linked to a filling and stabilization of charge trap states by photogenerated electrons; additionally, the long time constants associated with this process may indicate contributions from the slow motion of ions.[33,34] With higher Br-concentration (x = 0.6), the clear appearance of an additional higher wavelength emission peak is observed (Figure 2c and Supporting Information S6) and is attributed to formation of an I-rich phase with lower bandgap. However, the threshold for photoinduced halide segregation occurs at higher Br content in FACsPb-halide perovskites. In particular, the evolution of a second, long wavelength PL emission peak (I-rich phase) in FACs-perovskites appears to only evolve at Br compositions with $x \geq 0.5$ (Figure 2 and Supporting Information Figure S6). This is in agreement with literature, where for the specific composition of x = 0.4 a complete suppression of phase separation has been reported for FACs-, but not MA-perovskites (note: the power density in that study was as low as 0.03 suns whereas we use more than 10 times higher power density here).[26]

A notable difference between the materials studied here is that for the case of high Br content FACs-perovskites both the original and the emerging emission peaks (centered around 660−670 nm and 733−740 nm, respectively) increase in intensity with illumination time. In stark contrast, previous studies of $MAPb(I_{1-x}Br_x)_3$ films have shown an almost complete suppression of the short wavelength (i.e., the mixed

DOI: 10.1021/acs.nanolett.8b00541
Nano Lett. XXXX, XXX, XXX−XXX

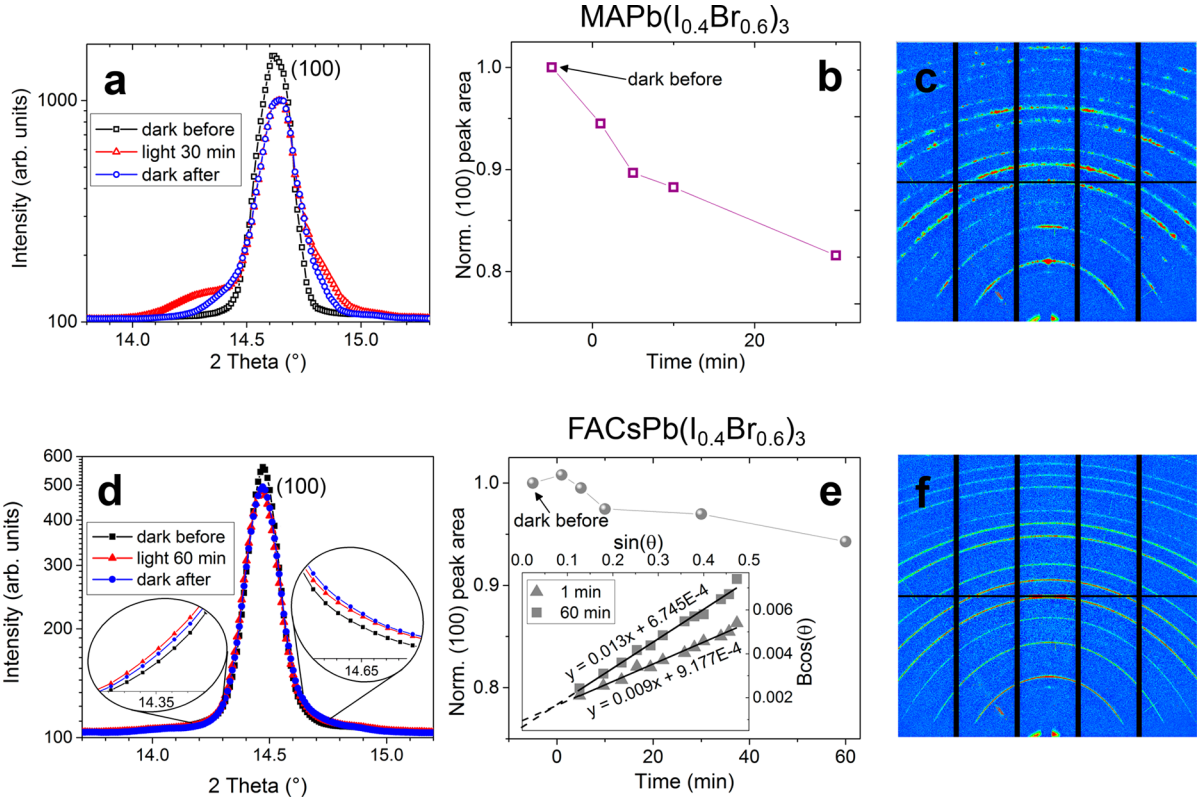

Figure 3. Synchrotron X-ray diffraction data and analysis of the (a–c) $MAPb(I_{0.4}Br_{0.6})_3$ and (d–f) $FACsPb(I_{0.4}Br_{0.6})_3$ samples. Both samples in cubic symmetry, indexing according to refs 11 and 41. (a,d) (100) diffraction peaks before illumination, during, and after relaxation in the dark. (b,e) Normalized peak area under illumination over time. The data points are connected as a guide for the eye. The inset in (e) shows the Williamson–Hall plot of the XRD peak fwhm (B) under illumination for 1 and 60 min. The points are fit with linear fits and equations are given. Dashed lines are the extension of the linear fits to the y-axis. (c,f) The 2D diffraction patterns after 30 and 60 min white light illumination, respectively.

I–Br phase) emission as the long wavelength I-rich PL emission increases to dominate the spectrum (see Supporting Information Figure S7).[12,35] The single PL emission in high Br-content MA-perovskites was explained by charge carriers that quickly reach the low bandgap I-rich regions, which act as the main radiative recombination sites.[16,36] In this respect, the difference between MA- and FACs-perovskites is surprising given that for both classes of material, PL emission energy differences between the original mixed I–Br phase and the newly formed I-rich domains is similar, suggesting similar energetic driving forces for charge localization, though the relative band offsets are not yet known. Furthermore, photocarrier diffusion lengths in both MAPb- and FACsPb-halides have been reported to be in the range of a few hundred nanometers to a few micrometers,[18,37] suggesting for both cation-compositions that they interact with large volumes of material, including regions of the newly formed I-rich phase. To gain more insights in the two phases that form under illumination, the Urbach energies of the original phase are compared to the formed phase(s) under illumination (Supporting Information Figure S8). There appears to be a small drop in Urbach energy upon illumination for $x = 0.2$ and 0.5, which implies reduced crystal lattice distortion caused by defects, dislocations, strain, and impurities. However, for higher Br-content, $x = 0.6$, the I-rich domain exhibits a significantly lower E_u compared to the original phase and the Br-rich domain. Although these findings are consistent with the improving PL efficiency with time, it remains surprising that PL from the wide bandgap phase is not quenched by charge injection and recombination in the lower bandgap phase, as is observed for MAPb-halide perovksites. Barker et al. explain the much higher PL signal of the I-rich phase compared to the mixed I–Br phase by reduced nonradiative recombination due to the accumulation of carriers in the low-bandgap regions leading to a significant local carrier enhancement[13] similarly, according to Tian et al., by funneling of charge carriers.[38] Consequently, the photoluminescence quantum yield from these regions is expected to be very high. This describes the behavior for both the MA- and FACs-perovskites, where there is significant growth of subgap PL emission. However, the PL growth of the high-energy peak in the FACs-perovskite cannot be described by this mechanism because funneling of charge carriers to the low bandgap region should (i) overall quench the PL by providing an alternative radiative recombination pathway and (ii) reduce the local carrier concentration such that the degree of state filling is lower and, thus, nonradiative recombination is more probable.

To summarize the in situ PL findings, the comparison of MA- versus FACs-perovskites indicates that both material classes exhibit photoinduced halide segregation at sufficiently high Br-concentration. For MA-perovskites, halide segregation results in quenching of emission from the mixed I–Br material and yields a single PL emission dominated by the I-rich phase, while in FACs-perovskites both the I-rich and mixed I–Br PL emission peaks increase in intensity with illumination time. The I-rich phases for the mixed FACs-halides have a similar emission peak centered around 740–750 nm (Supporting Information Figure S9).

DOI: 10.1021/acs.nanolett.8b00541
Nano Lett. XXXX, XXX, XXX–XXX

Another fundamental difference between MAPb-halides and FACsPb-halides is the changing crystal structure upon halide substitution. $MAPbI_3$ crystallizes in the tetragonal and $MAPbBr_3$ in the cubic structure,[11] while both iodide and bromide FA-perovskites adopt the cubic structure.[39,40] Previously, Barker et al. noted that for the MA-perovskite, the composition of the I-rich domains is $x = 0.2$, irrespective of the initial composition,[12] which is similar to the composition at which the stable phase changes from cubic to tetragonal. Therefore, they hypothesized that the I-enrichment could be limited to compositions of stable cubic phase because transformation to the tetragonal phase could introduce an energetic barrier to additional I-enrichment. However, our results suggest that such an explanation is unlikely because in FACs-perovskite all compositions are cubic and, nevertheless, the emission wavelength of the low-energy peak appears to be constant at ~740−750 nm (Figure 2 and Supporting Information Figures S6c and S9), which corresponds to $x \sim 0.2$, assuming any internal strain or quantum size effects in the newly formed phase are negligible. Thus, it appears that iodide enrichment occurs to a limiting composition even in the absence of crystal structure differences.

In order to provide additional insight into the underlying mechanisms of halide segregation and the effects of these processes on perovskite films, synchrotron X-ray diffraction was performed at the Advanced Light Source, beamline 12.3.2. Unlike conventional lab sources, synchrotron radiation has several orders of magnitude more flux and brilliance, allowing for significantly shorter collection times that enable in situ characterization of illumination-induced halide demixing. The grazing-angle geometry in combination with an area detector enables full XRD patterns to be recorded in the range of $5 < 2\theta < 57°$ within 60 s. Structural analysis of FACs- and MA-halide perovskite thin films (Figure 3) was performed under constant white light illumination with a Xe lamp at ~400 W/m^2 (see Supporting Information Figure S10 for lamp spectrum). In order to enable observation of diffraction peaks from both the original perovskite phase and of potential secondary phases that may evolve during halide demixing, we collected a wide range in 2θ spacing. In the following, we compare a MAPb- to a FACsPb-halide sample, both containing 60% bromide. Figures 3a,d show the (100) peaks of the $MAPb(I_{0.4}Br_{0.6})_3$ and $FACsPb(I_{0.4}Br_{0.6})_3$ samples, respectively. Measurements were collected before illumination, during illumination with the Xe lamp, and after ~7 min of relaxation in darkness. Full diffraction patterns can be found in the Supporting Information (Figure S11) and additional diffraction patterns with $x = 0.5$, 0.6, and 0.7 are provided in Figures S12 and S13.

Constant illumination of the MA-sample leads to a significant peak broadening and evolving peak asymmetry (Figure 3a), whereas the FACs-sample does not show a significant change in peak shape but does exhibit a slight broadening (illustrated by the zoomed insets in Figure 3d). The appearance of a new peak toward smaller angles observed in the MA-sample can be related to a new I-rich phase with different lattice parameters. More precisely, the PL peak emission of the I-rich phase in MA-perovskites is centered around 740 nm (Supporting Information Figure S14, and ref 12) and corresponds to a Br composition $x \sim 0.2$. Figure S14 in the Supporting Information suggests that the (100) XRD peak after 30 min of illumination is a convolution of an I-rich phase ($x \sim 0.2$) and a Br-rich phase ($x \sim 0.7$). This confirms previous measurements by Hoke et al. on MA-perovskites.[12] The photoinduced PL emission of the I-rich phase of the FACsPb-sample with $x = 0.6$ (before demixing) would correspond to an I-rich composition with $x = 0.2 - 0.3$. A change of $\Delta x = 0.3$ translates to a $\Delta(2\theta)$ of approximately 0.3° (peak position difference of the original I−Br phase to the I-rich phase with $x = 0.3$; compare Supporting Information Figure S5b), which is well within the instrument resolution. This reveals a significant difference between the MA- and the FACs-samples. Namely, there is halide demixing in both samples (seen in PL). However, while the I-rich phases structurally relax in the case of MA, they are not relaxed in FACs-perovskites. Simultaneously, the (100)-peak integrated intensity (peak area) of the $MAPb(I_{0.4}Br_{0.6})_3$ sample decreases by almost 20% within 30 min of constant illumination (Figure 3b) while the (100)-peak area of the $FACsPb(I_{0.4}Br_{0.6})_3$ sample drops by only ~5% within 60 min of illumination. This may be another indication of either loss of crystallinity or peak splitting caused by some statistically significant portion of the crystallites taking on a tetragonal symmetry upon illumination in the MA-samples. Please note the different time intervals of 30 and 60 min for the MA- and FACs-samples, respectively. Aside from broadening of existing peaks and the emergence of peaks indicating small changes of lattice spacing, no entirely new phases were observed. PbI_2 phase is present in our samples in the as-grown state as a consequence of the preparation process (see Figures S1 and S11 at ~12.7°).

A more rigorous and independent evaluation of the XRD peak broadening caused by domain size and strain was done by a Williamson-Hall plot (inset of Figure 3e).[42] The slope of a linear fit is equal to the strain and the grain size can be obtained from the intercept according to the equation $B\cos(\theta) = C\varepsilon\sin(\theta) + \frac{K\lambda}{L}$ with the integral line breath of the diffraction angle fwhm B (i.e., $B = \pi/2 \cdot$fwhm, fwhm for a Lorentzian peak fit), the Bragg angle as θ, the uncorrelated strain is ε, the X-ray wavelength is λ, the crystal grain diameter is L, and a proportionality constant is K which is 0.9 for roughly spherical crystal shape. The constant C is a proportionality factor between the apparent strain and the maximal strain and a typical value of 4 has been used here. The Williamson-Hall plot provides evidence that the FACs-sample is strained and the strain level increases during illumination (data depicted in Figure 3e; inset: 1 and 60 min illumination). Ion redistribution alone would lead to a change of the lattice parameter; the strain comes from the fact that the matrix surrounding the I-rich domains does not allow this new lattice parameter to be attained and instead the newly formed domains have lattice constants that are different than their relaxed values. Additionally, there can also certainly be inhomogeneous strain, as well as local distortions associated with halide distributions, and this would show up as broadening due to a distribution of lattice parameters (insets Figure 3d). Because of the asymmetry of the peaks, the noncontinuous Debye−Scherrer rings, and the transformation from cubic to tetragonal unit cell, it was not possible to fit the data of the MA-sample in a meaningful way.

The 2D diffraction patterns after white light illumination (Figures 3c,f) illustrate that FACs-perovskites exhibit continuous diffraction rings, reflecting small domain sizes, whereas the MA-perovskite patterns display distinct diffraction spots. The FACs-sample has a domain size in the 200 nm range (as determined from the Williamson-Hall plot analysis). It was not possible to extract the domain size of the MA-sample but the discontinuous Debye−Scherrer rings indicate domain size probably >500 nm. It appears that the halide demixing under

DOI: 10.1021/acs.nanolett.8b00541
Nano Lett. XXXX, XXX, XXX−XXX

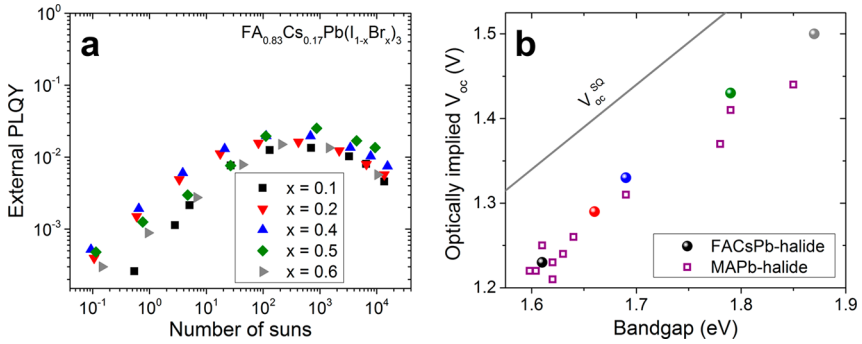

Figure 4. (a) PLQY of FACsPb$(I_{1-x}Br_x)_3$ thin films with $0.1 \leq x \leq 0.6$ at increasing illumination densities. (b) Implied V_{oc} versus bandgap of FACsPb- and MAPb- halide perovskite samples. The maximum achievable V_{oc}^{SQ} in the radiative limit is drawn as well (the optically implied V_{oc} values for MAPb-halides were taken from ref 35 and synthesized by LP-VASP process; experimental details can be found in SI).

illumination shown in the PL measurements (Figure 2) is reflected as a small peak broadening in the X-ray diffraction measurements but no diffraction peak asymmetry or evidence of peak splitting due to halide demixing as observed for the MA-sample. One suggestion to explain this finding is that I-rich domains nucleate in the FACs-sample, as evidenced from PL, but remain within individual grains by forming strained domains. The accumulation of stress may act as a stabilizing force against segregation.

PL measurements under continuous illumination (Figure 2) have shown that the dominant recombination processes for MA- and FACs-perovskites are very similar regarding the low-energy emission but not the high-energy emission. To shed further light on photocarrier recombination as a function of composition, we study the charge carrier injection-dependent recombination behavior by quantitative PL quantum yield measurements (PLQY). Two measurements on different spots were performed for each sample (Supporting Information Figure S15). Figure 4a shows the PLQY curves for FACsPb-$(I_{1-x}Br_x)_3$ thin films with $0.1 \leq x \leq 0.6$ versus the injected 1-sun equivalent illumination density. The trend for all Br-compositions is the same: increasing PLQY at low illumination densities up to ~100 suns where the external PLQY reaches a maximum of ~1%, followed by a PLQY drop at illumination densities ≳1000 suns. At illumination densities ~1-sun, samples with $x = 0.2$ and 0.4 exhibit the highest external PLQY, about 4 times higher than $x = 0.1$. We have previously reported similar results for the MAPb-halide perovskites.[35] A rise in PLQY at low excitation densities, as observed by multiple groups for MAPb-halide perovskites,[7,33,35,43,44] is characteristic of the filling of trap states with increasing optical generation rate until radiative recombination dominates.[33,43] At 1-sun, the performance of FACsPb-halides is limited by nonradiative trap-assisted recombination (due to fast carrier trapping), as is the case for MAPb-halides.[35,43,45]

Quantitative PLQY measurements allow for the extraction of the optically implied open-circuit voltage (V_{oc}) as a measure for the upper limit of the achievable V_{oc} purely based on material quality, circumventing contact formation[46,47]

$$qV_{oc} \approx kT \ln\left(\frac{J_{sc}}{J_0}\right) + kT \ln \mathrm{PLQY}_{ext} \quad (1)$$

$$kT \ln\left(\frac{J_{sc}}{J_0}\right) = V_{oc}^{SQ} \quad (2)$$

where V_{oc}^{SQ} is the V_{oc} in the Shockley-Queisser limit in which only interband radiative recombination occurs[48] and is approximated here as $E_g - 0.26$ eV,[49] J_{sc} is the short-circuit current density, and J_0 is the ideal reverse saturation current density for a given material. It is noted that PLQY_{ext} is a unitless quantity that by definition has a value that is ≤1. Figure 4b summarizes the implied V_{oc} calculated for MAPb- and FACsPb-halide perovskites with increasing bandgaps due to Br-alloying, which follow a linearly increasing behavior. The calculation is based on eq 1 and makes use of the maximum PLQY_{ext} that was measured typically for illumination densities >1 sun to illustrate the potential of lead halide perovskites. The implied V_{oc} for the same bandgap halide perovskite, but MA- versus FACs-cation is similar and slightly superior for FACs-perovskites with $E_g \geq 1.7$ eV. Thus, replacement of MA by FACs leads to enhanced stability without sacrificing the material quality.

In conclusion, mechanistic insights into the reduced photoinduced halide demixing in high Br-concentration FACs-perovskites were provided by combining PL and synchrotron X-ray diffraction measurements. For this study, the evolution of light-induced phase and composition changes in MA- and FACsPb-halide perovskites were directly compared. As a result, we find that FACsPb-halides do show light-induced halide demixing, which is accompanied by a very small XRD peak broadening, unlike significant peak broadening and splitting as observed in MA-perovskites. These results suggest that FACs-perovskites are unable to relax strain accumulated during halide demixing, as confirmed by the Williamson-Hall analysis, which could serve to partially stabilize the material against phase separation. Although the dominating recombination processes for the low-energy emission are similar for MA- and FACs-perovskites, the high-energy emission shows the opposite behavior. In particular, the emission is fully quenched in MA-perovskites but increases under illumination in FACs-perovskites. One hypothesis to explain this could be a reduction of nonradiative recombination centers in FACs-perovskites arising from the demixing process and buildup of strain. Beyond better stability, FACs-perovskites exhibit excellent intrinsic material properties as shown by PLQY measurements comparable to MA-perovskites. Our findings indicate the promise of FACsPb-halide perovskites as stable and efficient top cells for future photovoltaic tandem devices and provide insights into the factors affecting stability of high Br-concentration hybrid lead halide perovskites.

DOI: 10.1021/acs.nanolett.8b00541
Nano Lett. XXXX, XXX, XXX−XXX

■ ASSOCIATED CONTENT

Supporting Information

The Supporting Information is available free of charge on the ACS Publications website at DOI: 10.1021/acs.nanolett.8b00541.

Synthesis details, additional PL, synchrotron XRD, and PLQY data (PDF)

■ AUTHOR INFORMATION

Corresponding Authors

*E-mail: (C.M.S.-F.) csutterfella@lbl.gov.
*E-mail: (I.D.S.) sharp@wsi.tum.de.

ORCID

Carolin M. Sutter-Fella: 0000-0002-7769-0869
Camelia V. Stan: 0000-0002-5025-5568
Walter S. Drisdell: 0000-0002-8693-4562
Ian D. Sharp: 0000-0001-5238-7487

Author Contributions

The manuscript was written through contributions of all authors. All authors have given approval to the final version of the manuscript.

Notes

The authors declare no competing financial interest.

■ ACKNOWLEDGMENTS

This manuscript was prepared with support by the Solar Photochemistry Program of the U.S. Department of Energy, Office of Science, Office of Basic Energy Sciences, Division of Chemical, Geological and Biosciences under Contract No. DE-AC02-05CH11231. C.M.S.-F. acknowledges financial support from the Swiss National Science Foundation (fellowships P2EZP2_155586 and P300P2_171420). The photoluminescence measurements were supported by the Electronic Materials program, funded by the Director, Office of Science, Office of Basic Energy Sciences, Materials Sciences and Engineering Division of the U.S. Department of Energy under Contract No. DE-AC02-05CH11231. Synchrotron diffraction measurements were supported in part by the Joint Center for Artificial Photosynthesis, a DOE Energy Innovation Hub, supported through the Office of Science of the U.S. Department of Energy under Award Number DE-SC0004993. This research used beamline 12.3.2 at the Advanced Light Source, which is a DOE Office of Science User Facility under contract no. DE-AC02-05CH11231. K.L.G. was supported by the Cyclotron Road Applied Research Fellowship (DOE-EERE-RPP-AMO-2016) in partnership with Oak Ridge Institute for Science and Education (ORISE). I.D.S. acknowledges TUM.Solar in the context of the Bavarian Collaborative Research Project Solar Technologies Go Hybrid (SolTech). N.C. and F.M.T. acknowledge support from the Laboratory Directed Research and Development Program of Lawrence Berkeley National Laboratory under U.S. Department of Energy contract number DE-AC02-05CH11231, and from the CNR Program for Short Term Mobility.

■ REFERENCES

(1) Green, M. A.; Ho-Baillie, A.; Snaith, H. J. *Nat. Photonics* **2014**, *8*, 506−514.
(2) Park, N.-G. *Mater. Today* **2015**, *18*, 65−72.
(3) Stranks, S. D.; Snaith, H. J. *Nat. Nanotechnol.* **2015**, *10*, 391−402.
(4) Yin, W.-J.; Shi, T.; Yan, Y. *Appl. Phys. Lett.* **2014**, *104*, 063903.
(5) deQuilettes, D. W.; Koch, S.; Burke, S.; Paranji, R. K.; Shropshire, A. J.; Ziffer, M. E.; Ginger, D. S. *ACS Energy Lett.* **2016**, *1*, 438−444.
(6) Moser, J.-E. *Nat. Mater.* **2017**, *16*, 4−6.
(7) Richter, J. M.; Abdi-Jalebi, M.; Sadhanala, A.; Tabachnyk, M.; Rivett, J. P. H.; Pazos-Outón, L. M.; Gödel, K. C.; Price, M.; Deschler, F.; Friend, R. H. *Nat. Commun.* **2016**, *7*, 13941.
(8) Jacobsson, T. J.; Correa-Baena, J.-P.; Pazoki, M.; Saliba, M.; Schenk, K.; Grätzel, M.; Hagfeldt, A. *Energy Environ. Sci.* **2016**, *9*, 1706−1724.
(9) Duong, T.; Wu, Y.; Shen, H.; Peng, J.; Fu, X.; Jacobs, D.; Wang, E.-C.; Kho, T. C.; Fong, K. C.; Stocks, M.; et al. *Adv. Energy Mater.* **2017**, *7*, 1700228.
(10) Bush, K. A.; Palmstrom, A. F.; Yu, Z. J.; Boccard, M.; Cheacharoen, R.; Mailoa, J. P.; McMeekin, D. P.; Hoye, R. L. Z.; Bailie, C. D.; Leijtens, T.; et al. *Nature Energy* **2017**, *2*, 17009.
(11) Noh, J. H.; Im, S. H.; Heo, J. H.; Mandal, T. N.; Seok, S. I. *Nano Lett.* **2013**, *13*, 1764−1769.
(12) Hoke, E. T.; Slotcavage, D. J.; Dohner, E. R.; Bowring, A. R.; Karunadasa, H. I.; McGehee, M. D. *Chem. Sci.* **2015**, *6*, 613−617.
(13) Barker, A. J.; Sadhanala, A.; Deschler, F.; Gandini, M.; Senanayak, S. P.; Pearce, P. M.; Mosconi, E.; Pearson, A. J.; Wu, Y.; Srimath Kandada, A. R.; et al. *ACS Energy Lett.* **2017**, *2*, 1416−1424.
(14) Samu, G. F.; Janáky, C.; Kamat, P. V. *ACS Energy Lett.* **2017**, *2*, 1860−1861.
(15) Bischak, C. G.; Hetherington, C. L.; Wu, H.; Aloni, S.; Ogletree, D. F.; Limmer, D. T.; Ginsberg, N. S. *Nano Lett.* **2017**, *17*, 1028−1033.
(16) Slotcavage, D. J.; Karunadasa, H. I.; McGehee, M. D. *ACS Energy Lett.* **2016**, *1*, 1199−1205.
(17) Yoon, S. J.; Kuno, M.; Kamat, P. V. *ACS Energy Lett.* **2017**, *2*, 1507−1514.
(18) Rehman, W.; McMeekin, D.; Patel, J.; Milot, R.; Johnston, M.; Snaith, H.; Herz, L. *Energy Environ. Sci.* **2017**, *10*, 361−369.
(19) Han, Q.; Bae, S.-H.; Sun, P.; Hsieh, Y.-T.; Yang, Y. M.; Rim, Y. S.; Zhao, H.; Chen, Q.; Shi, W.; Li, G.; et al. *Adv. Mater.* **2016**, *28*, 2253−2258.
(20) Yi, C.; Luo, J.; Meloni, S.; Boziki, A.; Ashari-Astani, N.; Grätzel, C.; Zakeeruddin, S.; Röthlisberger, U.; Grätzel, M. *Energy Environ. Sci.* **2016**, *9*, 656−662.
(21) Jeon, N. J.; Noh, J. H.; Yang, W. S.; Kim, Y. C.; Ryu, S.; Seo, J.; Seok, S. I. *Nature* **2015**, *517*, 476−480.
(22) Binek, A.; Hanusch, F. C.; Docampo, P.; Bein, T. *J. Phys. Chem. Lett.* **2015**, *6*, 1249−1253.
(23) Yang, W. S.; Noh, J. H.; Jeon, N. J.; Kim, Y. C.; Ryu, S.; Seo, J.; Seok, S. I. *Science* **2015**, *348*, 1234−1237.
(24) Syzgantseva, O. A.; Saliba, M.; Grätzel, M.; Rothlisberger, U. *J. Phys. Chem. Lett.* **2017**, *8*, 1191−1196.
(25) Lee, J.-W.; Kim, D.-H.; Kim, H.-S.; Seo, S.-W.; Cho, S. M.; Park, N.-G. *Adv. Energy Mater.* **2015**, *5*, 1501310.
(26) McMeekin, D. P.; Sadoughi, G.; Rehman, W.; Eperon, G. E.; Saliba, M.; Hörantner, M. T.; Haghighirad, A.; Sakai, N.; Korte, L.; Rech, B.; et al. *Science* **2016**, *351*, 151−155.
(27) Li, W.; Wang, Z.; Deschler, F.; Gao, S.; Friend, R. H.; Cheetham, A. K. *Nature Reviews Materials* **2017**, *2*, 16099.
(28) Ono, L. K.; Juarez-Perez, E. J.; Qi, Y. *ACS Appl. Mater. Interfaces* **2017**, *9*, 30197−30246.
(29) Green, M. A.; Jiang, Y.; Soufiani, A. M.; Ho-Baillie, A. *J. Phys. Chem. Lett.* **2015**, *6*, 4774−4785.
(30) van Roosbroeck, W.; Shockley, W. *Phys. Rev.* **1954**, *94*, 1558−1560.
(31) Urbach, F. *Phys. Rev.* **1953**, *92*, 1324−1324.
(32) Sutter-Fella, C. M.; Miller, D. W.; Ngo, Q. P.; Roe, E. T.; Toma, F. M.; Sharp, I. D.; Lonergan, M. C.; Javey, A. *ACS Energy Lett.* **2017**, *2*, 709−715.
(33) Stranks, S. D.; Burlakov, V. M.; Leijtens, T.; Ball, J. M.; Goriely, A.; Snaith, H. J. *Phys. Rev. Appl.* **2014**, *2*, 034007.
(34) deQuilettes, D. W.; Zhang, W.; Burlakov, V. M.; Graham, D. J.; Leijtens, T.; Osherov, A.; Bulović, V.; Snaith, H. J.; Ginger, D. S.; Stranks, S. D. *Nat. Commun.* **2016**, *7*, 11683.

DOI: 10.1021/acs.nanolett.8b00541
Nano Lett. XXXX, XXX, XXX−XXX

(35) Sutter-Fella, C. M.; Li, Y.; Amani, M.; Ager, J. W.; Toma, F. M.; Yablonovitch, E.; Sharp, I. D.; Javey, A. *Nano Lett.* **2016**, *16*, 800−806.
(36) Draguta, S.; Sharia, O.; Yoon, S. J.; Brennan, M. C.; Morozov, Y. V.; Manser, J. M.; Kamat, P. V.; Schneider, W. F.; Kuno, M. *Nat. Commun.* **2017**, *8*, 200.
(37) Adhyaksa, G. W. P.; Veldhuizen, L. W.; Kuang, Y.; Brittman, S.; Schropp, R. E. I.; Garnett, E. C. *Chem. Mater.* **2016**, *28*, 5259−5263.
(38) Tian, W.; Leng, J.; Zhao, C.; Jin, S. *J. Am. Chem. Soc.* **2017**, *139*, 579−582.
(39) Weller, M. T.; Weber, O. J.; Frost, J. M.; Walsh, A. *J. Phys. Chem. Lett.* **2015**, *6*, 3209−3212.
(40) Hanusch, F. C.; Wiesenmayer, E.; Mankel, E.; Binek, A.; Angloher, P.; Fraunhofer, C.; Giesbrecht, N.; Feckl, J. M.; Jaegermann, W.; Johrendt, D.; et al. *J. Phys. Chem. Lett.* **2014**, *5*, 2791−2795.
(41) Baikie, T.; Fang, Y.; Kadro, J. M.; Schreyer, M.; Wei, F.; Mhaisalkar, S. G.; Graetzel, M.; White, T. J. *J. Mater. Chem. A* **2013**, *1*, 5628−5641.
(42) Williamson, G. K.; Hall, W. H. *Acta Metall.* **1953**, *1*, 22−31.
(43) Saba, M.; Cadelano, M.; Marongiu, D.; Chen, F.; Sarritzu, V.; Sestu, N.; Figus, C.; Aresti, M.; Piras, R.; Geddo Lehmann, A.; et al. *Nat. Commun.* **2014**, *5*, 5049.
(44) Deschler, F.; Price, M.; Pathak, S.; Klintberg, L. E.; Jarausch, D.-D.; Higler, R.; Hüttner, S.; Leijtens, T.; Stranks, S. D.; Snaith, H. J.; et al. *J. Phys. Chem. Lett.* **2014**, *5*, 1421−1426.
(45) Motti, S. G.; Gandini, M.; Barker, A. J.; Ball, J. M.; Srimath Kandada, A. R.; Petrozza, A. *ACS Energy Lett.* **2016**, *1*, 726−730.
(46) Ross, R. T. *J. Chem. Phys.* **1967**, *46*, 4590−4593.
(47) Smestad, G.; Ries, H. *Sol. Energy Mater. Sol. Cells* **1992**, *25*, 51−71.
(48) Shockley, W.; Queisser, H. J. *J. Appl. Phys.* **1961**, *32*, 510−519.
(49) Miller, O. D. Photonic Design: From Fundamental Solar Cell Physics to Computational Inverse Design. Ph.D. Thesis, University of California, Berkeley, California, 2012.

DOI: 10.1021/acs.nanolett.8b00541
Nano Lett. XXXX, XXX, XXX−XXX